PAPER

Check for updates

Tailored thermally stable functionalization of CsPbBr₃ nanocrystals for polymer nanocomposite scintillator fabrication

Jan Král, [ID] *[ab] Kateřina Děcká, [ID] [a] Petr Liška, [ID] [cd] Solangel Rojas Torres, [ID] [a]
Jan Valenta, [ID] [e] Vladimir Babin, [ID] [b] Ildefonso León Monzón, [ID] [f] Václav Čuba, [ID] [a]
Eva Mihóková [ID] [ab] and Etiennette Auffray [ID] [g]

CsPbBr₃ nanocomposites are prospective luminescent materials with great potential for many light-emitting applications. However, embedding CsPbBr₃ nanocrystals into some potentially interesting matrices proves challenging in terms of maintaining their properties and good transparency of the final nanocomposite, *e.g.*, high temperature polymerization of widely used and radiation-hard polystyrene or employment of more polar polymers such as polyurethanes often leads to nanocrystal degradation. Here, we present a functionalization strategy using ammonium hexafluorosilicate in combination with functional organosilanes for the fabrication of CsPbBr₃ nanocomposites, which provides improved thermal stability of surface passivation up to 110 °C. Moreover, it enables for the first time concomitant surface modification to enhance compatibility between nanocrystals and the matrix, leading to improved transparency of nanocomposites. We demonstrate that the process can be tailored by preparing polystyrene (PS) and polyurethane (PU) nanocomposites. This opens the way for easier processability of popular high cure temperature polymers such as polystyrene, as well as for efficient embedding of NCs into novel matrices with the aim of exploiting crucial properties for desired applications, for example, radiation hardness or flexibility.

Introduction

All-inorganic lead halide perovskite nanocrystals (NCs) with composition CsPbX₃ (X = Cl, Br, and I) are widely studied as bright luminescent materials with exciting properties for various light-emitting applications. In the past years, their narrow, spectrally tunable excitonic emission and also high atomic number have gained interest for radiation detection.[1–3] Fabrication of scalable nanoscintillators with tunable properties and dimensions by embedding these NCs into a polymer of the glass matrix is very attractive. Sharing with plastic scintillators the ease of processing and significantly lower cost compared to inorganic single crystals, they also provide superior stopping power and radiation hardness.[4–7] Moreover, their defect tolerance combined with potential quantum confinement effects leads to unique luminescent properties which promise to overcome the inherent limitations of traditional scintillating materials and open a way for novel performance possibilities and concepts. Their ultrafast multiexcitonic emission has shown prospective potential to substantially enhance the time-of-flight performance of medical imaging detectors[8] with possibilities for further exploitation of superradiant scintillation of single nanocrystals or their superlattices[9,10] with the aim of meeting the 10 ps challenge for time-of-flight positron emission tomography.[11] Among new concepts, recently proposed chromatic calorimetry can be named as a novel solution for high energy physics that takes advantage of the narrow emission peak of lead halide perovskite (LHP) NCs to construct a segmented detector capable of performing longitudinal tomography of the shower profile.[12]

However, embedding the LHP NCs into a matrix is not a trivial task. The main challenge is maintaining transparency while preserving the unique luminescence properties of the

a Faculty of Nuclear Sciences and Physical Engineering, Czech Technical University in Prague, Břehová 7, Prague, 115 19, Czech Republic.
E-mail: kralja13@fjfi.cvut.cz

b Institute of Physics of the Czech Academy of Sciences, Cukrovarnická 10, Prague, 162 00, Czech Republic

c Institute of Physical Engineering, Faculty of Mechanical Engineering, Brno University of Technology, Technická 2896/2, 616 69, Brno, Czech Republic

d Central European Institute of Technology, Brno University of Technology, Purkyňova 656/123, 612 00, Brno, Czech Republic

e Faculty of Mathematics and Physics, Charles University, Ke Karlovu 3, 121 16, Prague, Czech Republic

f Faculty of Physical-Mathematical Sciences, Autonomous University of Sinaloa, Culiacán, 80000, Mexico

g CERN, Esplanade des Particules 1, Meyrin, 1211, Switzerland

nanocrystal (NC) in the final nanocomposite (NCM); numerous approaches and strategies have been employed for the fabrication of nanocomposites (NCMs).[1,13,14] While glass nanocomposites now provide high photoluminescence (PL) quantum yields (QYs), homogeneous NC dispersion in the matrix and high chemical and photo-stability, embedding synthesized NCs into polymer matrices provides better control of NC properties resulting from colloidal synthesis, a more easily scalable method of nanocomposite fabrication with options of various shapes, coatings or other adaptable structures. In this work, we focus on the latter approach.

In addressing the polymer NCM transparency challenge, the copolymerization strategies using covalent bonding between the NC surface and the matrix were the most successful, reducing agglomeration of the NCs and achieving their more homogeneous dispersion in the matrix.[15–17] In terms of preservation of NC properties, photopolymerization and solvent evaporation proved to be gentler methods; however, they suffer from limitations in terms of loading and NCM dimensions.[18–21] However, thermal mass polymerization promises a technologically scalable method and allows for a high NC loading in the matrix (up to 40 wt%).[17] Moreover, thermal polymerization significantly broadens the options for matrix choice, especially polystyrene, which is a widely used polymer and exhibits the highest radiation hardness among ordinary industrial polymers.[5] However, thermal mass polymerization of styrene in the fabrication of the CsPbBr$_3$ NCM often leads to degradation of NC properties.[1,18] Temperatures at least above 60 °C are needed for the initiation of polystyrene-based polymers,[22] which can cause irreversible damage to NC properties due to ligand detachment, causing surface trap formation and nanocrystal aggregation.[6,23,24] Moreover, there exists a phase transition for CsPbBr$_3$ at around 88 °C[25] which, according to some authors,[6,26] could lead to the development of nonemissive allotropes.

Some works were successful in the preparation of CsPbBr$_3$ polystyrene NCMs while maintaining high PL QYs above 75%. Shi et al.[27] and Cai et al.[28] succeeded in producing efficient thin films of the CsPbBr$_3$ NCM by maintaining the polymerization temperature low at ≤60 °C. In addition, recently, Carulli et al.[6] presented fabrication of a defect-free CsPbBr$_3$ NCM by thermal polymerization of polyvinyl toluene at 65 °C using NCs passivated with didodecyldimethylammonium fluoride (DDAF). In all of these cases, the authors managed to preserve the luminescent properties of the NC because surface passivation was resistant to polymerization temperatures and prevented the desorption of ligands. The stable temperature of the ligand shell will become even more crucial and more difficult to achieve if one wishes to push the polymerization temperatures higher in order to achieve more efficient bulk polymerization or employ new matrices, e.g., transparent silicones.[29] The improved thermal resistance of the NC properties might also open up new NCM processing options, such as 3D printing.[30] In this regard, fluoride surface treatment emerges as the most promising approach. It was shown that pseudohalide anions such as ammonium hexafluorosilicate (AHFS)[31,32] or hexafluorophospate[32,33]

are prospective ligands achieving high PL QYs over 80%. Moreover, in the LED research on luminescence thermal quenching, it has been shown that fluoride treatment helps stabilize and suppress high temperature-induced ion migration in CsPbBr$_3$ NCs, while effectively passivating surface defects.[31,34–36] The translation of the advantages of this strategy into the fabrication of NCMs was demonstrated in the mentioned work by Carulli et al.[6] employing DDAF as the surface agent.

In this work, we present a novel process for the fabrication of a bright and transparent CsPbBr$_3$ polystyrene NCM. Using the AHFS passivation strategy,[31] for the first time for the fabrication of the NCM, we are able to reduce the thermal degradation of the NC properties to polymerization temperatures of up to 110 °C, temperatures far above previous works. Moreover, we are able to introduce additional allyl-functionalization of treated NCs to concurrently, for the first time, tackle the other challenge for NCM fabrication, namely the homogeneous NC dispersion in the matrix. Furthermore, we demonstrate that the AHFS passivation strategy with the consequent surface functionalization can be extended to a customized fabrication of NCMs with other polymers by preparing an amino-functionalized CsPbBr$_3$ NC embedded into polyurethane. We characterize the luminescence and scintillating properties of the prepared NCMs and assess their potential for novel applications in radiation detection.

Experimental

Chemicals

Acetone (p.a., P-LAB), ammonium hexafluorosilicate (AHFS, 98%, Thermo Scientific), allyltrimethoxysilane (ATMOS, 95%, Sigma-Aldrich), (3-aminopropyl)triethoxysilane (APTES, 99%, Sigma-Aldrich), 2,2′-azobis(2-methylpropionitrile) (AIBN, 98%, Sigma-Aldrich), Crystal Clear™ 202 EU (Smooth-On, Inc.), Cs$_2$CO$_3$ (99.9%, Sigma-Aldrich), ethyl acetate (p.a., PENTA), 1-octadecene (ODE, 90%, Sigma-Aldrich), oleic acid (OA, 90%, Sigma-Aldrich), oleylamine (OAm, 70%, Sigma-Aldrich), PbBr$_2$ (99.999%, Sigma-Aldrich), styrene (≥99.5%, Carl Roth), tetraethylorthosilicate (TEOS, ≥99.0% (GC), Sigma-Aldrich) and toluene (anhydrous, 99.8%, Sigma-Aldrich) were used. All chemicals were used as received without further purification unless otherwise stated.

CsPbBr$_3$ NC synthesis and modification

CsPbBr$_3$ NCs were prepared using a slightly modified original synthesis by Protesescu et al.[37] Cesium oleate was prepared using an increased 5 : 1 ratio of OA : Cs to be soluble at room temperature.[38] PbBr$_2$ was dissolved in octadecene using oleic acid (OA) and oleylamine (OAm) and dried, then pre-prepared cesium oleate was injected at 170 °C and subsequently the reaction was quenched after 10 seconds in an ice bath. The reaction mixture was then isolated by centrifugation at 10 950g for 5 minutes and the sediment was redispersed in toluene. Details about the synthesis can be found in the study of Děcká et al.[39]

To perform ligand exchange (LE), the AHFS powder was dissolved in water to obtain a 2 M solution. Then the AHFS solution was added to the NCs dispersed in toluene and the mixture was vigorously stirred for 5 minutes to increase the contact between the phases and enhance the effectiveness of LE. The ratio of 0.6 : 1 mg of AHFS in water and $CsPbBr_3$ NCs in toluene was used. We point out that to perform the ligand exchange effectively, the AHFS needs to be dissolved in water right before use, because of its hydrolysis (see the SI). The NCs treated with AHFS were then separated by centrifugation at 18 235g and redispersed again in toluene. The obtained solution was usually stirred in a vial for around 5 days prior to its use for the preparation of the NCM, to allow hydrolysis of AHFS to proceed.

For further surface functionalization of the AHFS-treated NCs, the solution of AHFS-treated NCs was stirred for one day after LE before the addition of the functional organosilane used for tailoring the NCs to the matrix. For allyl functionalization, 1 μL of ATMOS per 2.5 mg of $CsPbBr_3$ NCs was added under stirring and reacted for two days. Afterwards, the functionalized NCs were isolated by centrifugation and redispersed in a fresh solvent, either toluene for characterization or styrene for NCM preparation. To obtain amino-functionalized NCs for the polyurethane matrix, first 150 μL of TEOS was added to 7 mg of AHFS-treated $CsPbBr_3$ NCs in 1 mL of toluene. The solution was stirred and allowed to dry at 45 °C in a drying chamber. The SiO_2 encapsulated NCs were then redispersed in toluene by ultrasonication and 5 μL of (3-aminopropyl)triethoxysilane (APTES) was added for functionalization. The mixture was ultrasonicated for 5 minutes and then stirred for another 30 minutes. As-functionalized NCs in toluene were used for NCM fabrication.

Polymer nanocomposite preparation

In the preparation of polystyrene NCMs, functionalized NCs were dispersed in styrene to eliminate the adverse effects of toluene on the dispersion of NCs in the matrix.[17] First, the styrene monomer was purified from a polymerization inhibitor using an alumina column. Then, a viscous polystyrene prepolymer was produced by steady heating of the styrene monomer for about 30 minutes. Subsequently, the prepolymer was mixed with the colloidal NC solution and 0.3 wt% of the initiator azobisisobutyronitrile (AIBN). In this way, sedimentation of the NCs in the NCM is prevented and NC agglomeration is reduced compared with polymerization performed using pure styrene monomers. The polymerization reaction and hardening of the prepolymer mixture were then thermally reinitiated. The samples were heated either for 3 hours at 80 °C or for 45 minutes at 110 °C. For reference samples without exposure to increased temperatures, the mixture was left in the mold to harden at laboratory temperature for 14 days.

To prepare polyurethane NCM, Crystal Clear™ 202 EU, a commercial two-component urethane casting resin, was used. Aminofunctionalized NCs dispersed in toluene were added to component A containing 4,4′-methylenedicyclohexyldiisocyanate and mixed for about 5 minutes, and then the mixture was left at 45 °C to partially evaporate toluene and to react the surface amino groups of the NC with the isocyanate groups. Subsequently, component B was added in a 10A : 9B weight ratio and mixed well. The mixture was then poured into the mold and degassed for 5 minutes. Subsequently, the mold mixture was placed in a pressure chamber and allowed to cure at 3 bar pressure and laboratory temperature for two days.

Characterization methods

Infrared spectrometry was performed on an FT-IR spectrometer (NICOLET iS50, Thermo Scientific) using the attenuated total reflectance technique on a diamond crystal. For the measurement, the NCs were dropcast from the solution on an alumina plate, which was then placed on the crystal. The spectrum was acquired in the mid-infrared region (400–4000 cm^{-1}; resolution: 2 cm^{-1}) and subsequently processed with SW OMNIC 9 (Thermo Scientific). PL emission and transmittance spectra were obtained using a FluoroMax spectrofluorometer (Horiba Jobin Yvon). The PL emission of the NCs dispersed in toluene was excited at 320 nm, and the PL emission of the NCM was excited at 400 nm and collected in a reflectance configuration at a 45° angle between the sample and the incident beam. Radioluminescence (RL) spectra were obtained using a 5000 M spectrofluorometer (Horiba Jobin Yvon) with a monochromator, a TBX-04 photodetector (IBH Scotland) and a Seifert X-ray tube (40 kV, 15 mA) as the excitation source. All measurements were performed at laboratory temperature and in an ambient atmosphere.

For transmission electron microscopy (TEM), scanning transmission electron microscopy (STEM), and energy-dispersive X-ray (EDX) measurements, the NCs were dropcast from the solution on a TEM carbon film supported copper grid with standard thickness and grid size 400 mesh from Sigma-Aldrich. STEM micrographs were acquired on a focused ion beam/scanning electron microscope FEI Helios NanoLab 660 (HELIOS, Thermo Fisher Scientific) using an insertable STEM 3+ detector. Micrographs were recorded using high angle annular dark field imaging (HAADF) with a primary electron beam energy of 25 keV and a beam current of 25 pA. TEM micrographs were acquired using a low voltage electron microscope (LVEM 25E, Delong Instruments) with a primary electron beam energy of 25 keV. EDX analysis was performed in the STEM mode of LVEM 25E at 15 keV using the built-in Bruker Nano GmbH EDX detector XFlash 630, Mn FWHM 123.1 eV. The EDX spectrum was collected integrally over a rectangular area of 2 × 2 μm^2 (400 × 400 px^2) with a pulse throughput of 60 kcps using precise acquisition (250k counts, minor elements 1–10%), manual TEM background settings, Bayes deconvolution, and the Cliff-Lorimer quantification model.

The absolute PL QY was measured using a tuneable excitation source based on a Laser-Driven Light-Source LDLS (Energetiq) coupled to a 15-cm monochromator (Acton SP-2150i). The detection part consisted of a 30-cm imaging spectrograph (Acton SP-2300i) with an LN-cooled back-illuminated CCD camera (Spec-10:400B, Princeton Instruments). Samples were placed in a 50-mm integrating sphere (Thorlabs). Both the excitation and the

4442 | *J. Mater. Chem. C*, 2026, **14**, 4440–4450

This journal is © The Royal Society of Chemistry 2026

emission signals were coupled and guided using the silica fiber bundles. The set-up was absolutely calibrated using the secondary radiation standard (45 W tungsten–halogen lamp, Newport Oriel), and the estimated uncertainty of QY determination is 1–2% depending on the sample and spectral characteristics. For more details, refer to the study of Valenta and Valenta and Greben.[40,41]

The photoluminescence decay kinetics measurements at room temperature were performed using a FLUOROLOG-QM™ modular research fluorometer (Horiba Scientific). The excitation by 416 nm light was provided by pulsing the DeltaDiode laser head with a pulse duration below 100 ps. Emission at 515 nm was selected by the monochromator and registered using the time correlated single photon counting method (TCSPS) by the PMT R13456 (Hamamatsu). Fits of the decay curves were obtained by performing the convolution of the exponential function with the instrumental response and the least-square sum fitting procedure (SpectraSolve™ TM software package for Windows, Ames Photonics). The fast X-ray excited spectrally unresolved scintillation decays were measured at room temperature using a time-correlated single photon counting method using the FluoroHub unit coupled with a hybrid photomultiplier (Horiba Jobin Yvon) together with a picosecond X-ray pulsing source at 40 kV (Hamamatsu). The instrumental response function of the setup was 75 ps.

Results and discussion

NCs prepared using the hot injection method underwent an LE with AHFS (schematically depicted in Fig. 1(a)). As shown in Fig. 1(b), the FTIR spectra of the as-synthesized NCs exhibit dominant C–H stretching vibrations at 2920 and 2850 cm^{-1}. This signal is significantly reduced after the first LE cycle; meanwhile, new vibrations closely corresponding to the signal of pure AHFS powder appear, showing successful exchange of surface ligands. The bands at 3300–3030 and 1420 cm^{-1} are attributed to NH$_4^+$ stretching and bending vibrations, respectively,[42] and the bands at 710 and 475 cm^{-1} correspond to Si–F vibrations of the silicate anion.[43] To verify completeness of LE, a second cycle was performed, and no significant changes to the FTIR spectrum were observed, indicating complete surface saturation by SiF$_6^-$ and NH$_4^+$ ions after one LE cycle.

After LE, the NCs were stirred, and the FTIR spectra were evaluated over time. Zhang *et al.*[31] observed the appearance of Si–O–Si vibrations in FTIR spectra after two days and they ascribe it to the formation of a silica layer by slow hydrolysis of fluorosilicate, shown schematically in Fig. 1(c). From the FTIR results, we also observed the presence and slow growth of Si–O–Si vibrations over time, supporting the claim of silica layer formation (see Fig. 1(d)). When observing the STEM micrographs shown in Fig. 1(e), AHFS treated NCs with age did not show an observable silica shell; therefore, the formed surface silica probably exists in the form of a thin, close to the monomolecular layer, and no larger silica particle aggregates form. This agrees with the fact that we did not observe significantly improved resistance of as-treated NCs to exposure to water or other polar solvents, as the surface layer is too thin to provide necessary protection.

However, we propose that this thin layer can act as a platform for further modification of the NC surface using organosilane chemistry. As was shown, the surface fluorosilicate is
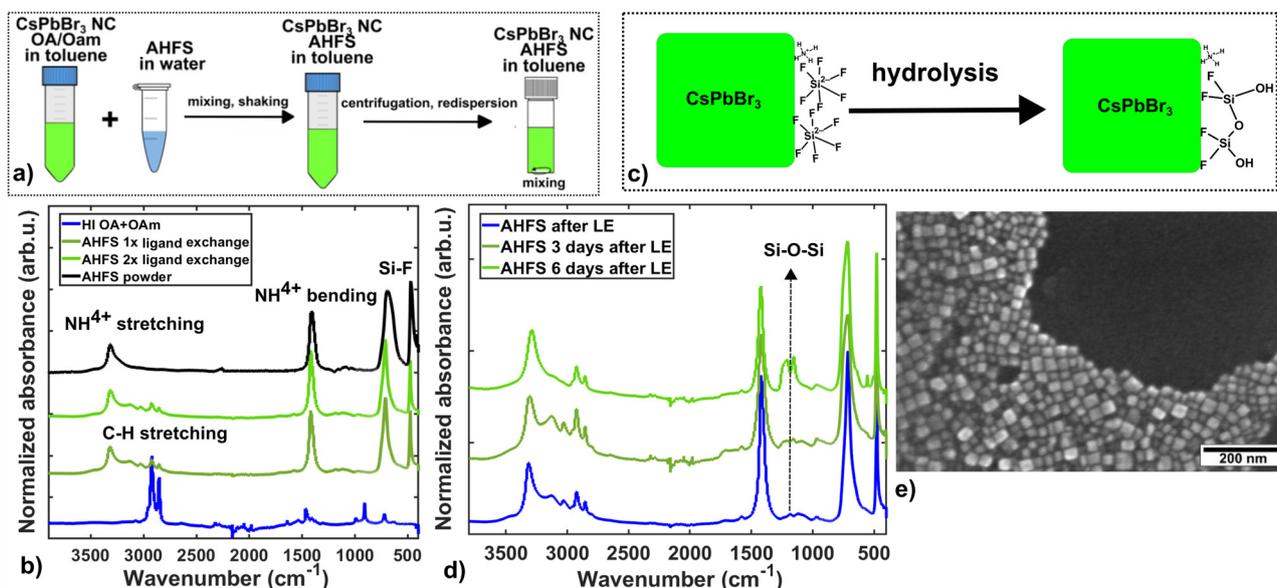

Fig. 1 (a) Schematic depiction of the AHFS LE cycle. (b) FTIR spectra of NCs as produced by the hot-injection method (blue), NCs after one cycle of AHFS LE (dark green), NCs after two cycles of AHFS LE (bright green) and pure AHFS powder (black). (c) Schematic depiction of siloxane bond formation on the NC surface by hydrolysis of AHFS over time. (d) FTIR spectra of NCs treated with AHFS after LE (blue) and the same sample after 3 days (dark green) and 6 days (bright green). (e) STEM micrograph of AHFS treated NCs.
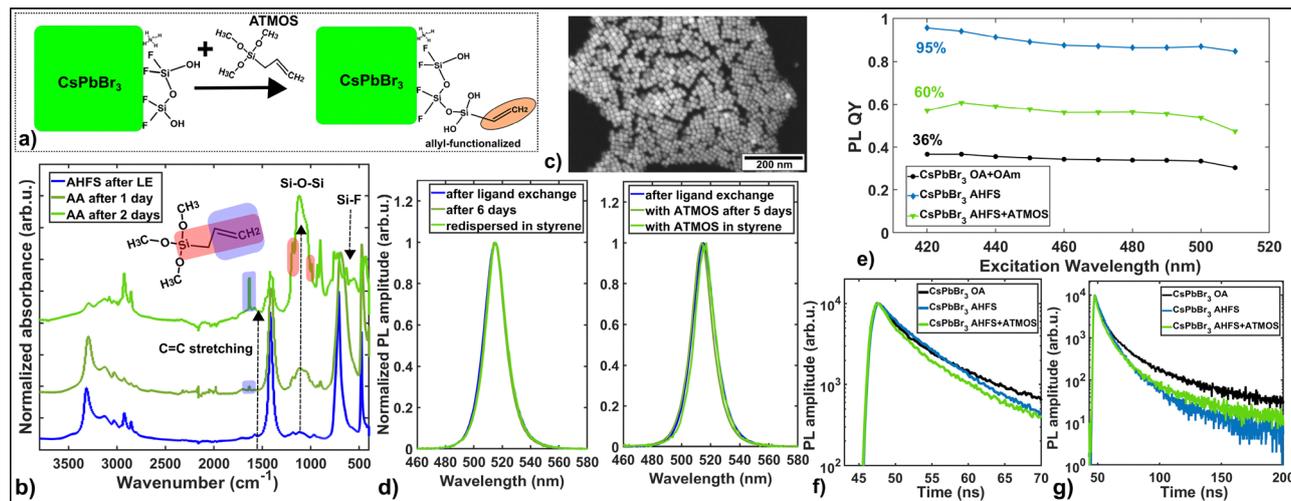
This journal is © The Royal Society of Chemistry 2026

J. Mater. Chem. C, 2026, **14**, 4440–4450 | **4443**

Fig. 2 (a) Schematic depiction of allyl-functionalization of AHFS treated NCs using ATMOS. (b) FTIR spectra of AHFS treated NCs after LE (blue) and the same NCs one day after addition of ATMOS to the solution (dark green) and two days after addition of ATMOS (bright green); the inset shows the molecular structure of ATMOS with highlighted bonds visible in the FTIR spectra. (c) STEM micrographs of allyl-functionalized AHFS treated NCs. (d) On the right, normalized PL spectra of AHFS treated NC solutions after LE (blue) and the same sample after 6 days (dark green) and redispersed in styrene before NCM preparation (bright green); on the left, normalized PL spectra of allyl-functionalized AHFS treated NC solutions after LE (blue) and the same sample after 5 days (dark green) and redispersed in styrene before NCM preparation (bright green). (e) PL QY values at various excitation wavelengths for NCs as produced by the hot-injection method (black), AHFS-treated NCs (blue) and allyl-functionalized NCs (bright green). (f) and (g) PL decay curves of NCs as produced by the hot-injection method (black), AHFS-treated NCs (blue) and allyl-functionalized NCs (bright green), shown in the short time scale and long time scale, respectively.

prone to hydrolysis, leading to the formation of silanol groups and siloxane bonding, which can be exploited to bring novel functionality to the surface by reacting it with functional organosilanes. To demonstrate this, we chose allyltrimethoxy-silane (ATMOS) as an agent for further functionalization. In our previous work,[17] we showed that allyl functionalization can be used to improve NC dispersion in the polystyrene matrix, leading to superior transparency of the resulting NCMs and allowing high NC loadings by copolymerizing with polystyrene. This modification is schematically depicted in Fig. 2(a).

Hence, ATMOS was added to the stirring AHFS-treated solution, and the reaction was evaluated over time. In this case, the Si-based network is formed faster compared to only the AHFS-treated sample, as demonstrated by the FTIR spectra in Fig. 2(b). Just after 2 days, the Si–O–Si band between 1000 and 1100 cm^{-1} is dominant, while there is a significant reduction in Si–F-based vibrations at 710 and 475 cm^{-1}. Meanwhile, the presence of C=C is evident by a narrow band at 1480 cm^{-1} as well as 1180 and 991 cm^{-1} vibration bands specific to the silicone-bound allyl group.[44] This suggests that the reaction between surface bound fluorosilicate anions and ATMOS was successful because ATMOS hydrolysis combined with more extensive Si–F hydrolysis produced a more extensive Si–O–Si network, and the presence of allyl vibrations shows a strong association of the organosiloxane polymers to the surface. Again, as treated NCs were observed by STEM, and no thick silica shell was observed, showing that the surface modification is still in the form of the ligand surface modification (see Fig. 2c). As functionalized NCs with AHFS and ATMOS in the work are denominated by the abbreviation AA.

During LE and organosilane functionalization, no significant changes to the PL profile were observed and the emission position was maintained as seen in Fig. 2(d). Importantly, a significant increase in PL QY was observed after LE (Fig. 2(e)), rising from 36% to 95% for excitation at 420 nm, pointing to nearly complete surface repassivation as the AHFS molecule can fill surface halide vacancies and repair the surface. A peel-off mechanism for this surface repair was proposed in the literature.[32] The subsequent allyl-functionalization led unfortunately to deterioration of the PL QY value to about 60%. Here, the decrease in surface passivation is probably due to the influence of released methanol during the hydrolysis of ATMOS. These results correspond well to observed PL kinetics. As seen in Fig. 2(f), the AHFS-treated sample exhibits the slowest first decay component corresponding to direct exciton recombination (4.24 ns, for the fitting, see the SI); meanwhile, both as-synthesized and allyl-functionalized NCs are influenced more extensively by non-radiative quenching, leading to acceleration of the decay component down to 3.69 ns and 3.04 ns, respectively. Looking at the slowest components (see Fig. 2(g)), both of these samples, especially as-synthesized NCs with OA and OAm, show increased presence due to the contribution of delayed recombination of surface trapped excitons and worse surface passivation.

Before embedding into polystyrene, functionalized NCs were transferred to styrene as a dispersion medium; the final spectra of NCs in styrene used for NCM fabrication are also shown in Fig. 2(d).

Polystyrene CsPbBr$_3$ nanocomposites

AHFS and allyl-functionalized AA NCs were embedded into polystyrene by thermally initiated polymerization with an AIBN

initiator as described in the Experimental section. To evaluate the suppression of thermal damage to the luminescent properties of NCs, a set of samples were prepared at various temperatures, namely 80 °C and 110 °C, to compare high temperature polymerization and 25 °C to have a reference sample not exposed to elevated temperatures. All samples were treated at respective temperatures till complete hardening, 3 hours for the 80 °C, 45 minutes for the 110 °C and 3 weeks for the 25 °C sample. We point out that even though it was possible to harden our polystyrene samples without thermal heating, it is not a scalable process, mostly limited by sample dimensions and long duration of hardening, necessitating thermal or other initiation of polymerization for practical sample production. In addition to various polymerization temperatures, the loading of NC in the matrix was varied for samples prepared at 80 °C in the range of 0.1 wt% to 10 wt% to observe the effect of higher NC concentrations.

However, first, the effect of allyl functionalization in AA samples was investigated compared to only AHFS-treated samples. As shown in Fig. 3(a), the transmittance of the A and AA samples prepared at 80 °C is compared at two sample thicknesses. Similarly to our previous work, significant improvement in NCM transparency is observed with additional allyl-functionalization of

the NCs, doubled for lower thickness at 525 nm from 5.7% to 11.4% and with its effect increasing with higher sample thickness as expected (more than 3× improvement from 1.9% to 6.4%). The generally low values of measured transmittance of the samples are, in our opinion, influenced by the long optical path of the spectrofluorimeter used for measurement, leading to rejection of nearly all scattered light. To provide a complete idea of the sample transparency, a photo of the sample is shown in the inset. Enhancing the transparency of the NCMs is crucial not only for an effective scintillating material but also generally for all light-emitting applications. Especially for prospective novel applications of cesium lead halide NCs in radiation detection, like chromatic calorimetry, the transmittance not only for emitted light but also to other wavelengths is necessary.

Showing that additional allyl-functionalization of AHFS NCs improves the NCM properties, the effect of fluoride surface treatment on the thermal stability of passivation is investigated on AA samples. The high temperature treatment affects the luminescence of $CsPbBr_3$ by ligand desorption and the consequent increase in surface trap density,[23] manifesting itself by a pronounced red shift in emission due to the recombination of shallowly trapped excitons.[4,26,45] For our samples, crucially, the spectral position and shape of the NCM samples remain
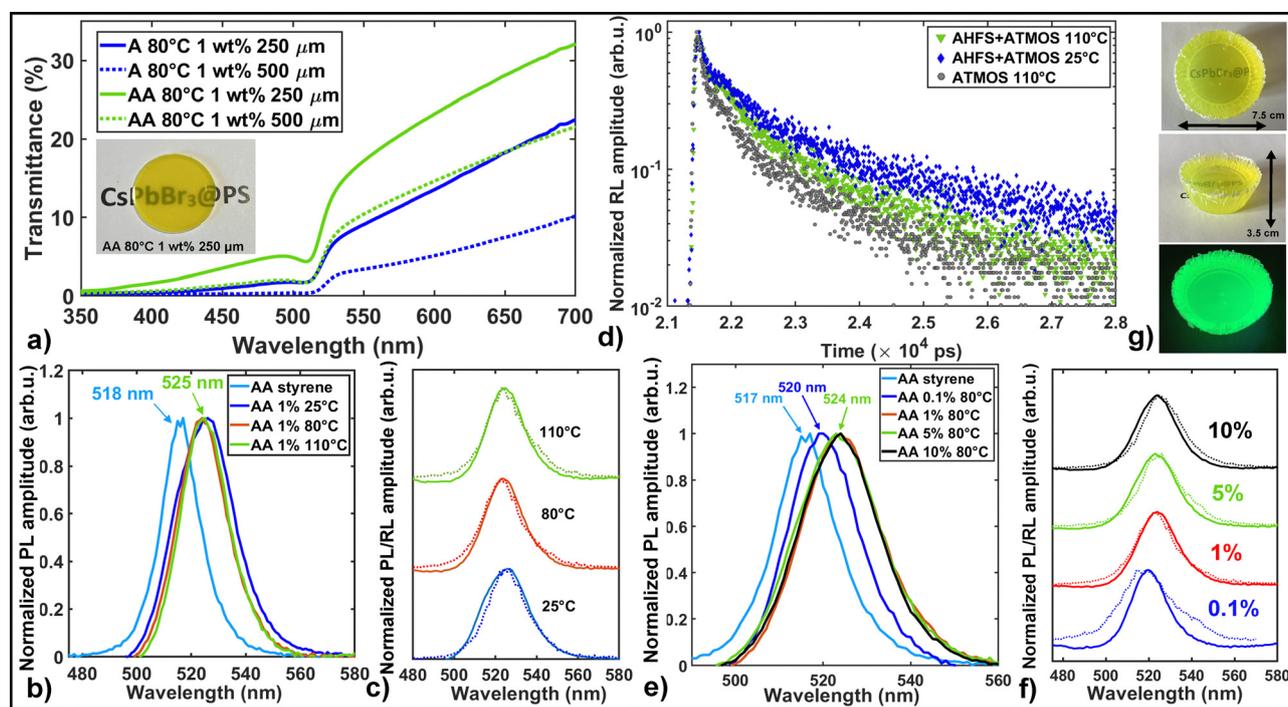

Fig. 3   (a) Transmittance spectra of the AHFS $CsPbBr_3$ NCM with 1 wt% loading prepared at 80 °C with 250 μm (blue solid) and 500 μm (blue dotted) thickness and of the allyl-functionalized AHFS $CsPbBr_3$ NCM with 1 wt% loading prepared at 80 °C with 250 μm (bright green solid) and 500 μm (bright green dotted) thickness; the inset shows a photo of the allyl-functionalized AHFS $CsPbBr_3$ NCM with 1 wt% loading prepared at 80 °C with 250 μm thickness. (b) Normalized PL spectra of the allyl-functionalized AHFS treated NC solution in styrene (light blue) and allyl-functionalized AHFS $CsPbBr_3$ NCM samples with 1 wt% loading prepared at 25 °C (dark blue), 80 °C (red) and 110 °C (bright green). (c) Normalized PL (solid line) and RL (dotted line) spectra of the same NCM samples as in (b). (d) RL decay curves of the allyl-functionalized AHFS $CsPbBr_3$ NCM with 1 wt% loading prepared at 25 °C (blue diamonds) and 110 °C (bright green triangles) and the NCM sample with NCs functionalized only with ATMOS prepared at 110 °C (grey circles). (e) Bulk allyl-functionalized AHFS $CsPbBr_3$ NCM with 0.03 wt% loading prepared at 80 °C. (f) Normalized PL spectra of the allyl-functionalized AHFS treated NC solution in styrene (light blue) and the allyl-functionalized AHFS $CsPbBr_3$ NCM with 0.1 wt% (dark blue), 1 wt% (red), 5 wt% (bright green) and 10 wt% (black) loading prepared at 80 °C. (g) Normalized PL (solid line) and RL (dotted line) spectra of the same NCM samples as in (f).

This journal is © The Royal Society of Chemistry 2026

J. Mater. Chem. C, 2026, **14**, 4440–4450 | **4445**

unchanged with an increase in the polymerization temperature from 25 °C to 110 °C. The PL spectra of the respective AA NCM samples are shown in Fig. 3(b) alongside the AA styrene precursor solution for NCM preparation. The emission maximum of all NCMs is red-shifted compared to the precursor solution by 7 nm, probably because of enhanced reabsorption due to the much higher concentration of NCs in the medium. Fig. 3(c) shows a comparison of the PL spectra with the respective RL spectra, and here again we can observe the unaltered position and shape of the emission with increasing polymerization temperature, showing no red-shift due to recombination of shallow trapped excitons, pointing to the stability of the ligand shell to high temperature polymerization. To further investigate the suppression of thermal damage by AHFS surface passivation, the RL decay kinetics of the samples are compared as shown in Fig. 3(d) (the fitted data can be found in the SI) with the sample produced with ATMOS-only treated NCs prepared as in our previous work.[17] The difference between the samples is in slow components, where the acceleration of the kinetics can be ascribed to increased luminescence quenching from surface traps and an enhanced contribution of shallow exciton recombination. Here, the impact of increased polymerization temperature on the decay profile is observable. The reference sample prepared at 25 °C exhibits the slowest decay. Even though the AHFS-treated sample prepared at 110 °C shows accelerated decay with respect to the reference, there is still significant improvement compared to the sample not passivated with fluorides featuring the fastest decay of all. This might suggest that the ligand shell stability is improved and stable to high temperatures, even though the trap formation is probably not entirely prevented, and in order to fully suppress it, the polymerization temperature might need to be lowered. However, the red-shift due to shallow exciton recombination was not observed in the emission spectra and the reason for observed quenching might be instead the formation of nonemissive allotropes due to phase transition[6,25,26] and energy transfer to them.[46] Regardless, the AHFS treatment seems to provide improved thermal stability to the ligand shell and is able to produce a bright sample even with preparation at 110 °C. Crucially, the perspective sub-nanosecond components of multi-excitonic origin are produced in the samples by high density excitation of X-rays.

In addition, the effect of increasing loading on the spectral position and shape was investigated. In Fig. 3(e), the PL spectra of NCMs with loading between 0.1 wt% and 10 wt% are shown, and Fig. 3(f) shows a comparison of the PL spectra with the corresponding RL spectra of the respective samples. In the PL spectra, we observe a gradual red shift of the emission from the precursor styrene solution to the NCM with 0.1 wt% loading and to NCM with 1 wt% loading, attributable to the increasing effect of emission reabsorption due to increasing NC concentration. However, further increase of the NC loading from 1 wt% to 10 wt% leads to no additional redshift which might be due to saturation of reabsorption at the concentration level where all short-wavelength light gets effectively reabsorbed. Importantly, the emission spectra of the NCs with AHFS

passivation are unaltered even at high concentrations. At these levels of loading, NC aggregation at elevated temperatures might have become more pronounced, leading to further red-shift of the emission.[23] Here, apart from the improved temperature stability of the ligand shell, thanks to AHFS, the allyl-functionalization with ATMOS is probably also essential, improving NC dispersion in the matrix, reducing agglomeration of the NCs to clusters and mitigating their aggregation as was shown in our previous work.[17] Finally, our protocol was then scaled with success to bulk samples, and the NCM with 0.03 wt% loading and centimeter scale dimension is shown in Fig. 3(g).

Therefore, both functionalities of our novel combination of thermal stability enhancement fluoride treatment together with the copolymerization strategy to improve NC dispersion were successfully demonstrated, showing their advantage for polystyrene NCM preparation over only fluoride treatment using organic ligands like DDAF[6] or only copolymerizable ligands like ATMOS.[17] However, the advantage of AHFS treatment of NCs is not limited only to polystyrene NCM preparation. Thanks to its compatibility with organosilane chemistry, we suggest the protocol can be successfully modified to suit also other polymer matrices, where by changing the functional group of the organosilane used, the NC modification can be tailored to the specific chemistry of the matrix, providing again robust passivation of the NC surface as well as superior NC dispersion in the matrix. This brings an opportunity for research on different polymers to exploit improved or novel NCM properties like radiation hardness or flexibility. Moreover, this whole process is post-synthetic, which means it can be easily scaled and adapted to $CsPbBr_3$ NCs synthesized using larger-scale methods compared to the hot-injection synthesis.[47] Therefore, the process can be exploited not only in scintillation applications, such as chromatic calorimetry,[12] but also in other light emitting applications. To demonstrate the possibility of tailoring the process for different polymer matrices, AHFS treated NCs were embedded into the polyurethane matrix. We chose polyurethane because it is another popular polymer with versatile properties and applications[48] and can be engineered to be both flexible and radiation resistant.[49,50]

Polyurethane $CsPbBr_3$ nanocomposites

To embed the AHFS NCs into a polyurethane matrix, the functionalization process was modified. First of all, solely AHFS treated NCs could not be embedded into polyurethane since the polar hydroxy and isocyano groups of polyurethane precursors caused fast NC decomposition upon addition. The insufficient protection of AHFS from polar environments again points to mono- or nearly monomolecular surface passivation. To increase the resistance of as passivated NCs, the surface protection layer of NCs was first enhanced by growing a larger SiO_2-based shell by adding tetraethoxysilane (TEOS) and subsequently functionalized with (3-aminopropyl)triethoxysilane (APTES), providing an NH_2 functional group able to co-react with isocyanate groups of polyurethane precursors.[51] The described process is schematically depicted in Fig. 4(a).
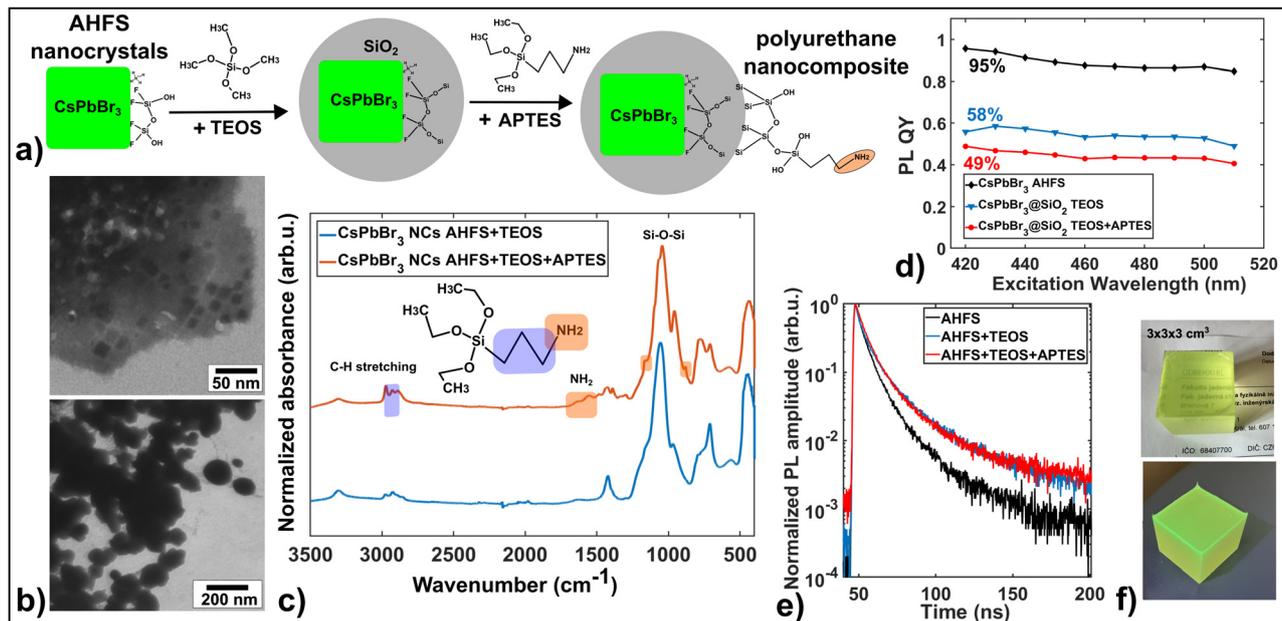
4446 | *J. Mater. Chem. C*, 2026, **14**, 4440–4450

This journal is © The Royal Society of Chemistry 2026

Fig. 4 (a) Scheme of AHFS treated NC functionalization for polyurethane NCMs. (b) TEM micrographs of SiO_2 encapsulated AHFS treated NCs. (c) FTIR spectra of SiO_2 encapsulated AHFS $CsPbBr_3$ NCs before (blue) and after (light red) APTES functionalization. (d) PL QY values for AHFS-treated NCs (black), SiO_2 encapsulated NCs (blue) and amino-functionalized NCs (red). (e) PL decay curves for the same samples as in (d). (f) Photos of the $CsPbBr_3$ polyurethane NCM with 0.05 wt% loading, under ambient light (above) and under UV light (below).

The AHFS NCs encapsulated in SiO_2 by TEOS are observed from the TEM micrographs shown in Fig. 4(b). We claim that the NCs are fully or partially encapsulated in SiO_2, since there are several images indicating the presence of preserved NCs in a thin electron beam transmissible layer (<100 nm, upper image) attached to wider corpuscles (lower image) that are no longer transmissible by electrons ($\gg100$ nm). Upon close examination by EDX, we confirm that the wider corpuscles consist of SiO_2 and contain Cs, Pb, and Br as evidence of the presence of $CsPbBr_3$ NCs. For more detailed analysis and discussion of the measured composition of particles, see the SI.

The FTIR spectra shown in Fig. 4(c) are dominated by Si–O–Si vibrations at 1000–1100 cm^{-1}); however, after APTES functionalization, new weak vibrations attributable to the presence of the NH_2 and CH_2 groups of APTES are identified. The vibrations at 1485 and 1560 cm^{-1} with the shoulder around 1645 cm^{-1} correspond to characteristic vibrations of the $-NH_3^+-HCO_3$ salt, which is formed by reaction of the NH_2 group with carbon dioxide and water when the 3-aminopropyl compounds are hydrolyzed in air.[44] Since we handled the sample for FTIR measurements in air, this reaction was likely to occur. In addition, two peaks at 1165 and 880 cm^{-1} similar to specific ATMOS vibrations appear in the spectra and might be attributed to the $Si-(CH_2)_3-NH_2$ structure. Moreover, a relative increase in CH stretching vibrations is observed, providing further evidence of the successful functionalization of the surface of APTES.

The advantage of SiO_2 shell growth from AHFS treated NCs might be the growth of the SiO_2 network directly from the NC surface, thanks to the presence of AHFS, leading to better

preserved surface passivation compared to protocols using organic ligands[52] and decreased NC agglomeration in the SiO_2 shell. Nevertheless, the PL QY of the encapsulated NCs did decrease to 58% during the process (see Fig. 4(d)), the reasons being probably the same as with the allyl-functionalization, the release of alcohols during the hydrolysis, in this case, of ethanol. The subsequent amino-functionalization by APTES of silica encapsulated NCs decreased their PL QY only mildly since they were protected by the shell from the additional products of APTES hydrolysis. The PL QY measurements are complemented by PL decay curves in Fig. 4(e) showing identical presence of slower components for both TEOS encapsulated and APTES functionalized NCs, attributable to delayed recombination of trapped excitons, pointing to minor influence of further functionalization after encapsulation. In the future, the layer thickness and SiO_2 particle size might be optimized by varying the TEOS amount and the TEOS : APTES ratio to enable higher NC loading in the matrix at the same transparency level.

The as prepared NCs were then embedded into polyurethane without heating, as described in the Experimental section. The resulting transparent $3 \times 3 \times 3$ cm^3 cubic NCM sample with a loading of 0.05 wt% is shown in Fig. 4(f) with the corresponding PL and RL spectra in Fig. 5(a). Both the emission maxima of 515 nm and the spectral shape are maintained for the precursor toluene solution and the RL of the NCM. In the RL spectra, emission of the PU matrix is also intense (a broad band centered around 425 nm), as most of the X-ray energy is deposited in the matrix due to the low NC concentration. With increasing NC content, the ratio of energy deposited in NC would grow and also more of the PU light would get reabsorbed
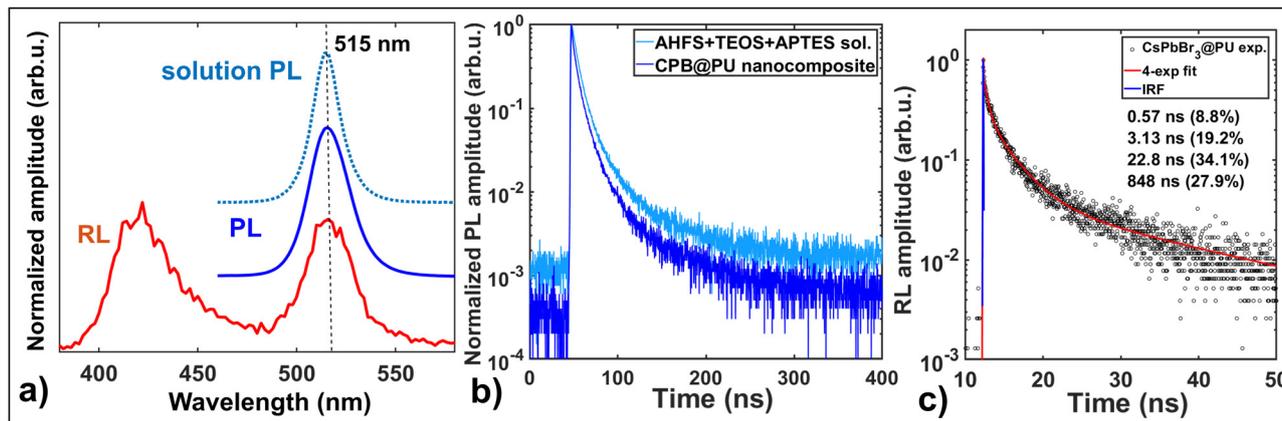
This journal is © The Royal Society of Chemistry 2026

J. Mater. Chem. C, 2026, **14**, 4440–4450 | **4447**

Fig. 5 (a) Normalized PL spectra of AHFS treated NCs in the toluene precursor solution and normalized PL and RL spectra of the CsPbBr$_3$ polyurethane NCM. (b) PL decay curves for the amino-functionalized NCs in toluene (light blue) and the same NCs embedded into PU (dark blue). (c) RL decay curve of the CsPbBr$_3$ PU NCM, the experimental data are shown as black circles, the 4-exponential fit is shown as a red line and IRF is in blue, and the fitted parameters are shown in the inset.

and reemitted by NCs, providing improved scintillating properties of the NCM. The decay kinetics of the embedded NCs were well preserved as well. PL decay curves in Fig. 5(b) do not show any additional slow components, suggesting that no new surface traps were introduced during nanocomposite fabrication. Additionally, in the RL decay curves (see Fig. 5(c)), an ultra-fast multi-excitonic component is present even at these low levels of loading, suggesting that there is sufficient energy deposition in the NCs. Although not fully optimized, we were able to successfully adapt our fluoride passivation process to the polyurethane matrix, showing the potential and significant advantages of our approach of using AHFS as a platform for functionalization of the CsPbBr$_3$ NCs, tailorable to matrix chemistry, leading to enhanced performance of NCMs.

Summary and conclusions

We have successfully prepared polystyrene and polyurethane CsPbBr$_3$ NCMs with preserved luminescent properties. We show that using AHFS represents a prospective surface passivation strategy, providing improved thermal stability of the ligand shell as well as an option for additional functionalization to tailor the NCs for improved NC dispersion in the polymer matrix. The enhanced thermal resistance to 110 °C of our passivated CsPbBr$_3$ NCs enables fast and efficient fabrication of bright polystyrene NCMs, even though the effects of thermal polymerization are not suppressed entirely and to produce completely defect-free NCMs, the polymerization temperature might need to be lowered. Anyway, this high-temperature process opens up possibilities for the search for novel matrices with higher processing temperatures, such as siloxanes, or new processing methods, such as 3D printing. Moreover, it might be used to improve the compatibility of the NCs with other commonly used polymers through a tailored surface, thereby leading to enhancements in their transparency. This potential for tailoring the functionalization process was demonstrated by preparing polyurethane CsPbBr$_3$ NCMs.

Author contributions

Jan Král: conceptualization, formal analysis, investigation, validation, visualization, methodology, writing – original draft, and writing – review & editing. Kateřina Děcká: conceptualization, supervision, and writing – review & editing. Petr Liška: investigation, writing – original draft, and writing – review & editing. Solangel Rojas Torres: investigation and writing – review & editing. Jan Valenta: investigation, formal analysis, and writing – review & editing. Vladimir Babin: investigation, formal analysis, and writing – review & editing. Ildefonso León Monzón: conceptualization and writing – review & editing. Václav Čuba: conceptualization, funding, resources, project administration, supervision, and writing – review & editing. Eva Mihóková: conceptualization, funding, resources, project administration, supervision, and writing – review & editing. Etiennette Auffray: conceptualization, funding, resources, project administration, supervision, and writing – review & editing.

Conflicts of interest

There are no conflicts to declare.

Data availability

Supplementary information (SI) is available. Supplementary information contains fitted photoluminescence and radioluminiscence decay curves of the nanocrystals at different stages of the functionalization and fitted decay curves of the prepared nanocomposites. Addtionally, it contains elementary composition of CsPbBr$_3$@SiO$_2$ particles based on EDX spectrum, data on influence of AHFS hydrolysis on ligand exchange and study of long-term stability of the nanocomposite photoluminiscence. See DOI: https://doi.org/10.1039/d5tc03614c.

4448 | *J. Mater. Chem. C*, 2026, **14**, 4440–4450

This journal is © The Royal Society of Chemistry 2026

Acknowledgements

References

1 A. Anand, M. L. Zaffalon, A. Erroi, F. Cova, F. Carulli and S. Brovelli, *ACS Energy Lett.*, 2024, **9**, 1261–1287.

2 A. Antonelli, E. Auffray, S. Brovelli, F. Bruni, M. Campajola, S. Carsi, F. Carulli, G. De Nardo, E. Di Meco, E. Diociaiuti, A. Erroi, M. Francesconi, I. Frank, S. Kholodenko, N. Kratochwil, E. Leonardi, G. Lezzani, S. Mangiacavalli, S. Martellotti, M. Mirra, P. Monti-Guarnieri, M. Moulson, D. Paesani, E. Paoletti, L. Perna, D. Pierluigi, M. Prest, M. Romagnoni, A. Russo, I. Sarra, A. Selmi, F. Sgarbossa, M. Soldani, R. Tesauro, G. Tinti and E. Vallazza, *Nucl. Instrum. Methods Phys. Res., Sect. A*, 2024, **1069**, 169877.

3 Q. Chen, J. Wu, X. Ou, B. Huang, J. Almutlaq, A. A. Zhumekenov, X. Guan, S. Han, L. Liang, Z. Yi, J. Li, X. Xie, Y. Wang, Y. Li, D. Fan, D. B. L. Teh, A. H. All, O. F. Mohammed, O. M. Bakr, T. Wu, M. Bettinelli, H. Yang, W. Huang and X. Liu, *Nature*, 2018, **561**, 88–93.

4 M. L. Zaffalon, F. Cova, M. Liu, A. Cemmi, I. Di Sarcina, F. Rossi, F. Carulli, A. Erroi, C. Rodà, J. Perego, A. Comotti, M. Fasoli, F. Meinardi, L. Li, A. Vedda and S. Brovelli, *Nat. Photonics*, 2022, **16**, 860–868.

5 F. Markley, D. Woods, A. Pla-Dalmau, G. Foster and R. Blackburn, *Radiat. Phys. Chem.*, 1993, **41**, 135–152.

6 F. Carulli, A. Erroi, F. Bruni, M. L. Zaffalon, M. Liu, R. Pascazio, A. El Adel, F. Catalano, A. Cemmi, I. Di Sarcina, F. Rossi, L. Lazzarini, D. E. Manno, I. Infante, L. Li and S. Brovelli, *ACS Energy Lett.*, 2024, **10**, 12–21.

7 H. Zhang, Z. Yang, M. Zhou, L. Zhao, T. Jiang, H. Yang, X. Yu, J. Qiu, Y. M. Yang and X. Xu, *Adv. Mater.*, 2021, **33**, 2102529.

8 F. Pagano, J. Král, K. Děcká, M. Pizzichemi, E. Mihóková, V. Čuba and E. Auffray, *Adv. Mater. Interfaces*, 2024, **11**, 2300659.

9 M. L. Zaffalon, A. Fratelli, Z. Li, F. Bruni, I. Cherniukh, F. Carulli, F. Meinardi, M. V. Kovalenko, L. Manna and S. Brovelli, *Adv. Mater.*, 2025, **37**, 2500846.

10 G. Rainò, M. A. Becker, M. I. Bodnarchuk, R. F. Mahrt, M. V. Kovalenko and T. Stöferle, *Nature*, 2018, **563**, 671–675.

11 P. Lecoq, *IEEE Trans. Radiat. Plasma Med. Sci.*, 2017, **1**, 473–485.

12 Y. Haddad, D. Arora, E. Auffray, M. Doser, M. Salomoni and M. Weber, Quantum Dot Based Chromatic Calorimetry: A proposal, *arXiv*, 2025, preprint, arXiv:2501.12738, DOI: 10.48550/arXiv.2501.12738, https://arxiv.org/abs/2501.12738.

13 A. Soosaimanickam, P. J. Rodríguez-Cantó, J. P. Martínez-Pastor and R. Abargues, in *Preparation and processing of nanocomposites of all-inorganic lead halide perovskite nanocrystals*, Elsevier, 2021, pp. 19–93.

14 S. Samiei, J. Lin, E. Soheyli, G. Nabiyouni and D. Chen, *Adv. Opt. Mater.*, 2025, **13**, 2500162.

15 A. Pan, Y. Zhou, C. Zhao, C. Shi, Y. Wu, Y. Zhang, Y. Liu and L. He, *Chem. Eng. J.*, 2022, **433**, 133590.

16 H. Kim, S. So, A. Ribbe, Y. Liu, W. Hu, V. V. Duzhko, R. C. Hayward and T. Emrick, *Chem. Commun.*, 2019, **55**, 1833–1836.

17 J. Král, K. Děcká, V. Zabloudil, P. Liška, F. Hájek, M. Horák, V. Čuba, E. Mihóková and E. Auffray, *J. Phys.*, 2024, **8**, 015007.

18 Y. Xin, H. Zhao and J. Zhang, *ACS Appl. Mater. Interfaces*, 2018, **10**, 4971–4980.

19 A. Erroi, S. Mecca, M. L. Zaffalon, I. Frank, F. Carulli, A. Cemmi, I. Di Sarcina, D. Debellis, F. Rossi, F. Cova, K. Pauwels, M. Mauri, J. Perego, V. Pinchetti, A. Comotti, F. Meinardi, A. Vedda, E. Auffray, L. Beverina and S. Brovelli, *ACS Energy Lett.*, 2023, **8**, 3883–3894.

20 K. Děcká, F. Pagano, I. Frank, N. Kratochwil, E. Mihóková, E. Auffray and V. Čuba, *J. Mater. Chem. C*, 2022, **10**, 12836–12843.

21 X. Jia, T. Shi, Q. Zhang, H. Huang, P. K. Chu, X.-F. Yu and R. He, *Chem. Eng. J.*, 2024, **500**, 156756.

22 T. Pirman, M. Ocepek and B. Likozar, *Ind. Eng. Chem. Res.*, 2021, **60**, 9347–9367.

23 B. T. Diroll, G. Nedelcu, M. V. Kovalenko and R. D. Schaller, *Adv. Funct. Mater.*, 2017, **27**, 1606750.

24 X. Yuan, X. Hou, J. Li, C. Qu, W. Zhang, J. Zhao and H. Li, *Phys. Chem. Chem. Phys.*, 2017, **19**, 8934–8940.

25 M. Rodová, J. Brožek, K. Knížek and K. Nitsch, *J. Therm. Anal. Calorim.*, 2003, **71**, 667–673.

26 F. Cova, A. Erroi, M. L. Zaffalon, A. Cemmi, I. Di Sarcina, J. Perego, A. Monguzzi, A. Comotti, F. Rossi, F. Carulli and S. Brovelli, *Nano Lett.*, 2024, **24**, 905–913.

27 S. Shi, L. Cao, H. Gao, Z. Tian, W. Bi, C. Geng and S. Xu, *Nanoscale*, 2021, **13**, 9381–9390.

28 Y. Cai, P. Zhang, W. Bai, L. Lu, L. Wang, X. Chen and R.-J. Xie, *ACS Sustainable Chem. Eng.*, 2022, **10**, 7385–7393.

29 Y. Zhang, X. Yang, X. Zhao and W. Huang, *Polym. Int.*, 2012, **61**, 294–300.

This journal is © The Royal Society of Chemistry 2026

J. Mater. Chem. C, 2026, **14**, 4440–4450 | **4449**

30 C.-L. Tai, W.-L. Hong, Y.-T. Kuo, C.-Y. Chang, M.-C. Niu, M. Karupathevar Ponnusamythevar Ochathevar, C.-L. Hsu, S.-F. Horng and Y.-C. Chao, *ACS Appl. Mater. Interfaces*, 2019, **11**, 30176–30184.

31 Q. Zhang, Z. Li, M. Liu, L. Kong, W. Zheng, B. Wang and L. Li, *J. Phys. Chem. Lett.*, 2020, **11**, 993–999.

32 X. Shen, S. Wang, X. Zhang, H. Wang, X. Zhang, C. Wang, Y. Gao, Z. Shi, W. W. Yu and Y. Zhang, *Nanoscale*, 2019, **11**, 11464–11469.

33 K. Xie, S. Zhang, X. Wang, C. Gong, C. Zheng, W. Xiao and F. Li, *J. Lumin.*, 2022, **252**, 119401.

34 M. Liu, Q. Wan, H. Wang, F. Carulli, X. Sun, W. Zheng, L. Kong, Q. Zhang, C. Zhang, Q. Zhang, S. Brovelli and L. Li, *Nat. Photonics*, 2021, **15**, 379–385.

35 M. Liu, Q. Wan, X. Liao, W. Zhan, C. Yuan, Q. Zhang, M. He, C. Zou, M. Pan, L. Kong and L. Li, *J. Mater. Chem. C*, 2023, **11**, 10965–10972.

36 Q. Zhang, M. He, Q. Wan, W. Zheng, M. Liu, C. Zhang, X. Liao, W. Zhan, L. Kong, X. Guo and L. Li, *Chem. Sci.*, 2022, **13**, 3719–3727.

37 L. Protesescu, S. Yakunin, M. I. Bodnarchuk, F. Krieg, R. Caputo, C. H. Hendon, R. X. Yang, A. Walsh and M. V. Kovalenko, *Nano Lett.*, 2015, **15**, 3692–3696.

38 C. Lu, M. Wright, X. Ma, H. Li, D. Itanze, J. A. Carter, C. Hewitt, G. Donati, D. Carroll, P. Lundin and S. Geyer, *Chem. Mater.*, 2018, **31**, 62–67.

39 K. Děcká, J. Král, F. Hájek, P. Průša, V. Babin, E. Mihóková and V. Čuba, *Nanomaterials*, 2021, **12**, 14.

40 J. Valenta, *Nanosci. Methods*, 2014, **3**, 11–27.

41 J. Valenta and M. Greben, *AIP Adv.*, 2015, **5**, 047131.

42 J. Pironon, M. Pelletier, P. De Donato and R. Mosser-Ruck, *Clay Miner.*, 2003, **38**, 201–211.

43 R. Stodolski and L. Kolditz, *J. Fluorine Chem.*, 1985, **29**, 73.

44 P. Launer and B. Arkles, Infrared Analysis of Organosilicon Compounds, in *Silicon Compounds: Silanes & Silicones*, Gelest Inc., 2013.

45 C. Rodà, M. Fasoli, M. L. Zaffalon, F. Cova, V. Pinchetti, J. Shamsi, A. L. Abdelhady, M. Imran, F. Meinardi, L. Manna, A. Vedda and S. Brovelli, *Adv. Funct. Mater.*, 2021, **31**, 2104879.

46 T. Noblet, J. Hottechamps, M. Erard and L. Dreesen, *J. Phys. Chem. C*, 2022, **126**, 15309–15318.

47 S. Wang, A. A. Yousefi Amin, L. Wu, M. Cao, Q. Zhang and T. Ameri, *Small Struct.*, 2021, **2**, 2000124.

48 H. Engels, H. Pirkl, R. Albers, R. W. Albach, J. Krause, A. Hoffmann, H. Casselmann and J. Dormish, *Angew. Chem., Int. Ed.*, 2013, **52**, 9422–9441.

49 J. Wang, Y. Tu, X. Zhang and S. Guo, *Polymer*, 2023, **289**, 126485.

50 J. Wang, S. Guo and X. Zhang, *Macromolecules*, 2024, **57**, 11266–11275.

51 M. Rostami, Z. Ranjbar and M. Mohseni, *Appl. Surf. Sci.*, 2010, **257**, 899–904.

52 C. K. Trinh and Z. Ahmad, *R. Soc. Open Sci.*, 2024, **11**, 230892.